Proceedings of the ASME 2010 3rd Joint US-European Fluids Engineering Summer Meeting and 8th International Conference on Nanochannels, Microchannels, and Minichannels
FEDSM-ICNMM2010
August 1-5, 2010, Montreal, Canada

FEDSM-ICNMM2010-30593

NUMERICAL ASSESSMENT OF THE QUASI-STEADY APPROXIMATION IN GLOTTAL AIR FLOW

Hani Bakhshaei
Department of Mechanical Engineering
McGill University
Montreal, Quebec, Canada

Luc Mongeau
Department of Mechanical Engineering
McGill University
Montreal, Quebec, Canada

Rosaire Mongrain
Department of Mechanical Engineering
McGill University
Montreal, Quebec, Canada

ABSTRACT

Voice production involves air flow through the glottis and its interaction with the deformable vocal folds. The quasi-steady approximation involves modeling the complex unsteady flow through the glottis as a sequence of steady flows through rigid orifices, which is numerically less expensive. Theoretical and experimental assessments of the quasi-steady approximation have been attempted, but contradictions in previously reported results prompt further analysis. To investigate the validity of the quasi-steady approximation, a two-dimensional dynamic simulation of air flow through an idealized glottal orifice with moving walls was performed for different pressure gradients and oscillation frequencies. A series of steady flow simulations for configurations of the vocal folds and flow boundary conditions that instantaneously coincide with data from the dynamic simulations were performed. Dynamic and static simulations were performed using the COMSOL multiphysics® software. Both stationary and non-stationary geometries were created based on the M5 model with the orifice profile alternating between convergent and divergent included angles (-40° to 40°). The distance between the vocal cord tip and the centerline was established to maintain a constant vocal fold volume, thereby eliminating spurious monopole sources. The results include the fluid flow rate, the pressure drop across the glottis, the shear stress on the glottis walls, and the orifice coefficient. Comparison between these variables for both dynamic and static sets of data allowed the assessment of the accuracy of the quasi-steady approximation to predict the fluid flow in the glottis. The importance of time-dependent terms over short intervals during glottal opening and closure was scrutinized. The results may contribute to the general goal of creating flow models that are optimal for laryngeal orifice coefficient and sound pressure determination.

INTRODUCTION

Voice production or phonation, involves air flow through the glottis and its interaction with the deformable vocal folds. As a result of fluid-structure interactions during phonation, the vocal folds undergo three dimensional oscillations at frequencies around 100 Hz[1].

Computer simulations of the air flow within the glottis, the vocal fold oscillations and their interactions provide a better understanding of voice production which is useful for clinical applications in speech sciences[2]. For example physiological models of speech production which are based on articulatory parameters may someday help to assess the possible consequences of phonosurgery on a patient's voice pre-operatively [2]. Because the creation of realistic models of the vocal folds that describe the complex aspects of the oscillations is computationally expensive, some simplification assumptions are needed. Canonical two-dimensional geometries of the glottis[3, 4], the quasi-steady approximation of air flow in glottis[2, 5, 6], and driven models of vocal cords[7, 8], have

been used. In the present study, a two-dimensional, driven, computational model of the larynx was used to evaluate the validity of the quasi-steady approximation.

The quasi-steady approximation in fluid dynamics models unsteady fluid flow through a time-varying orifice as a series of steady flows through fixed orifices with configurations and boundary conditions that are instantaneously the same as the time-varying cases at specific time values. In other words, the contribution of time dependent terms in the equation of motion is assumed to be negligible. The quasi-steady approximation may lead to significantly decreased computational costs through the conversion of a dynamic problem into a sequence of static problems. Experimental verifications of this approximation have been reported. Zhang *et al*. [2] built a dynamic mechanical model of the larynx and investigated the range of validity of the quasi-steady approximation. Dynamic results were compared to predictions based on the quasi-steady approximation. A good agreement between the two sets of data was obtained in different ranges of operating frequencies, flow rates and orifice shapes. It was concluded that the quasi-steady approximation is valid for the tonal component of sound generated by pulsating confined jets. Vilain *et al*. [5] presented a theoretical description of the flow through the glottis based on quasi-steady boundary layer theory, along with experimental verifications of the quasi-steady approximation. In contrast, theoretical and experimental studies have reported that unsteady fluid flow effects are significant and time dependent terms cannot be ignored. Krane *et al*. [9] in a theoretical assessment of aerodynamic effects in phonation have identified two temporal regimes. The first one is dominated by the unsteady effects, local fluid acceleration and acceleration induced by the vocal fold walls. The second temporal regime is the interval in which flow obeys a quasi-steady behavior[9]. Measurements of fluid flow through a scaled-up model of human glottis have been done by Krane *et al*. [10] to investigate the unsteady behavior of glottal flow. According to this study, the flows through the moving vocal cords and the nonmoving glottis exhibit significant differences.

Further work seems to be warranted. In the present study, the quasi-steady approximation was evaluated using a two-dimensional computational flow model. This paper is organized as follows. Background on the dynamic and static model set up, such as the glottal geometry, finite element simulation methods and boundary conditions are presented. In the result and discussion section, results of dynamic simulations of air flow within the glottis at different frequencies and pressure gradients are shown and compared with corresponding steady state solutions. The influence of wall motion on the pressure gradient across the glottis, the flow rate, the stress on the vocal fold surface and the flow orifice coefficient was quantified through comparisons between static and dynamic solutions.

NOMENCLATURE

F	Body force*(N)*
P	Pressure *(Pa)*
S	Shear stress (N/m^2)
T	Period of oscillation *(s)*
Ψ	Orifice angle *(°)*
ω	Frequency of oscillation *(Hz)*
ρ	Density(Kg/m^3)
μ	Dynamic viscosity($Pa.s$)
A_m	Minimum area of the glottis(m^2)
u_m	Centerline velocity at minimum area of the glottis(*m/s*)
Q_{real}	Real flow rate (m^3/s)
Q^{dy}	Flow rate-Dynamic simulation (m^3/s)
Q^{st}	Flow rate-Static simulation (m^3/s)
C_d^{dy}	Orifice coefficient-Dynamic simulation
C_d^{st}	Orifice coefficient-static simulation

DYNAMIC SIMULATIONS

Geometry of Vocal Fold With Constant Area

To define the two-dimensional profile of the glottis, the M5 model [3] was used. In this model, shown in Fig. 1, the orifice angle (Ψ) varies between -40° to 40° for convergent and divergent orifice shapes respectively.

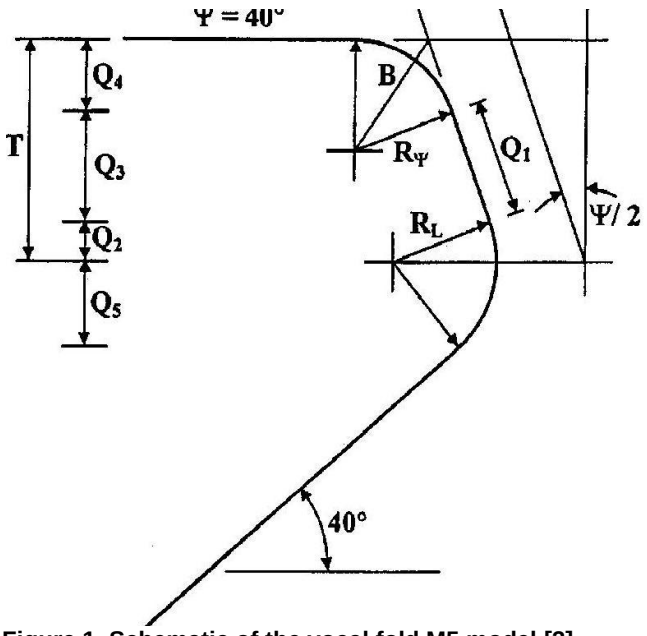

Figure 1. Schematic of the vocal fold M5 model [3]

The surface area was kept constant in order to avoid volume variations of the solid material. The vocal fold tissue is generally considered to be incompressible because of its large water content. One complete cycle of vocal fold oscillations is defined as the motion from an orifice included angle equal to $\Psi = -40°$ to 40° and the subsequent return to the initial configuration($\Psi = -40°$). This cycle is divided into 40 different steps. At each time step, the area of the vocal cord is calculated and compared to the area at $\Psi = -40°$ which was

selected as the baseline. For each configuration, the profile is translated along the transverse (Y) direction until the area reaches the same value as for $\Psi = -40°$. The upper tip (referred to as point A) shifting is illustrated in Fig. 2. The end points (Points B and C) are fixed. Five different glottal configurations with constant area are shown in Fig. 2.

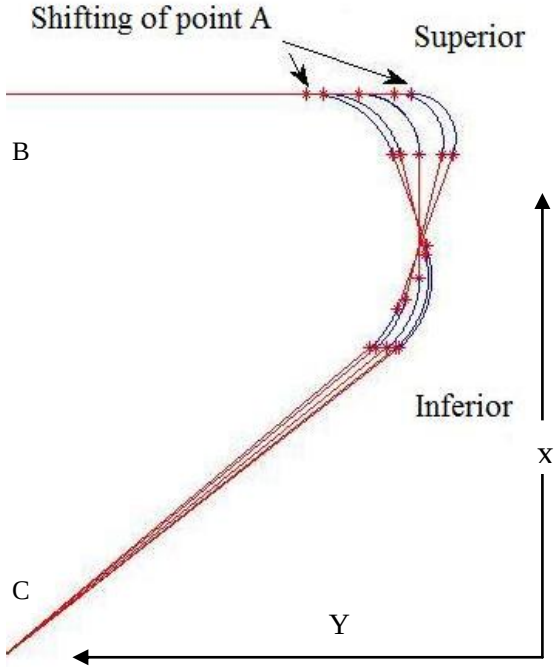

Figure 2. Evolution of the glottal orifice profile geometry over one cycle

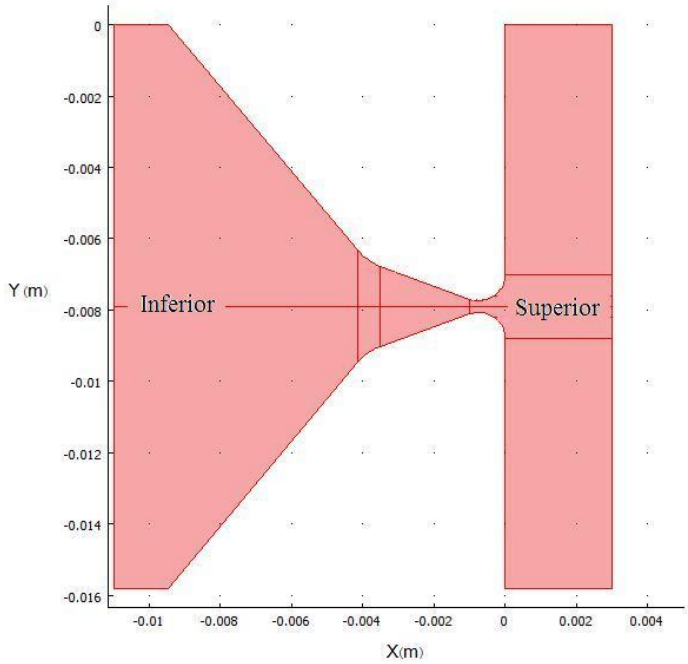

Figure 3. Computational domain

The surface area of the vocal folds model was constant for all values of the orifice angle. The coordinate translation procedure establishes the distance between the vocal cord tip and the centerline automatically. It should be pointed out that the orifice never closed completely to avoid mesh collapse. That could result in a reduction of the contribution of the unsteady terms, which tend to dominate at opening and closure.

Numerical Procedure For the Dynamic Model

Dynamic simulations were performed using the commercially available software COMSOL. Figure. 3 shows the geometry of the computational domain.

Although the orifice geometry is symmetric with respect to the centerline, the flow simulations were performed for the entire orifice consisting of two identical vocal cords. No symmetry boundary condition was applied on the centerline. This allows the capture of asymmetric effects in the flow field. It is worth mentioning that the two vocal folds are assumed to have the same geometry. Small differences between the right and left vocal fold have been reported in the literature[4].

The fluid flow was considered to be incompressible and laminar. The Mach number based on the maximum velocity in the glottis was M≈0.1 and the Reynolds number was still in the laminar regime Re <2500. The Navier-Stokes and the continuity equations was solved using the COMSOL multiphysics® software.

$$\rho(\boldsymbol{u}\cdot\nabla)\boldsymbol{u} = \nabla\cdot[-P\boldsymbol{I} + \boldsymbol{\mu}(\boldsymbol{\nabla u} + (\boldsymbol{\nabla u})^{T})] + F$$
$$\nabla\cdot\boldsymbol{u} = \boldsymbol{0} \qquad (1)$$

The gauge pressure magnitude was imposed at inlet and outlet boundaries. In the time-dependent simulations, the inlet pressure was gradually ramped up from a zero amplitude at a constant rate to the desired value. The outlet pressure was set to be $P = 0$. To handle the moving wall problem, the moving mesh application mode was used. The Moving Mesh application in COMSOL is based on the Arbitrary Lagrangian Eulerian (ALE) method. Further details on the (ALE) method can be found in the COMSOL documentation and other sources [11, 12]. In the Moving Mesh mode, the mesh movement in the horizontal and vertical directions must be defined at the boundaries. As described in the previous section, the position of all the points in the M5 model may be obtained as of time functions. Regression functions were used to define the motion of vocal cords at boundaries. At the start and end point of each segment on one boundary, the regression functions yield the horizontal and vertical components of the mesh movement. For points in between, linear interpolation of the start and the end point motions are used. To achieve a smooth surface over the entire oscillation cycle, the regression function curves along the superior and inferior tips were divided into 4 and 8 segments, respectively.

The computational domain was divided into different subdomains as illustrated in Fig.3 .The type and size of the mesh defined separately in each of the subdomains. Domain positioning enables a finer mesh in subdomains near the

constriction walls, and a coarser mesh in other subdomains. Constraints at the interfaces also prevent the mesh from collapsing and getting inverted. In moving boundary problems with large deformations, the mesh elements may get inverted which may decrease the accuracy of the solution and in extreme cases cause divergence. The use of interfacial constraints at the boundaries results in less mesh deformation and better convergence of the solution. Other factors such as the smoothing method, the mesh type, the solution tolerance and the remeshing algorithm have effects on the convergence of the solution. More detailed information about these parameters is available in the software documentation.

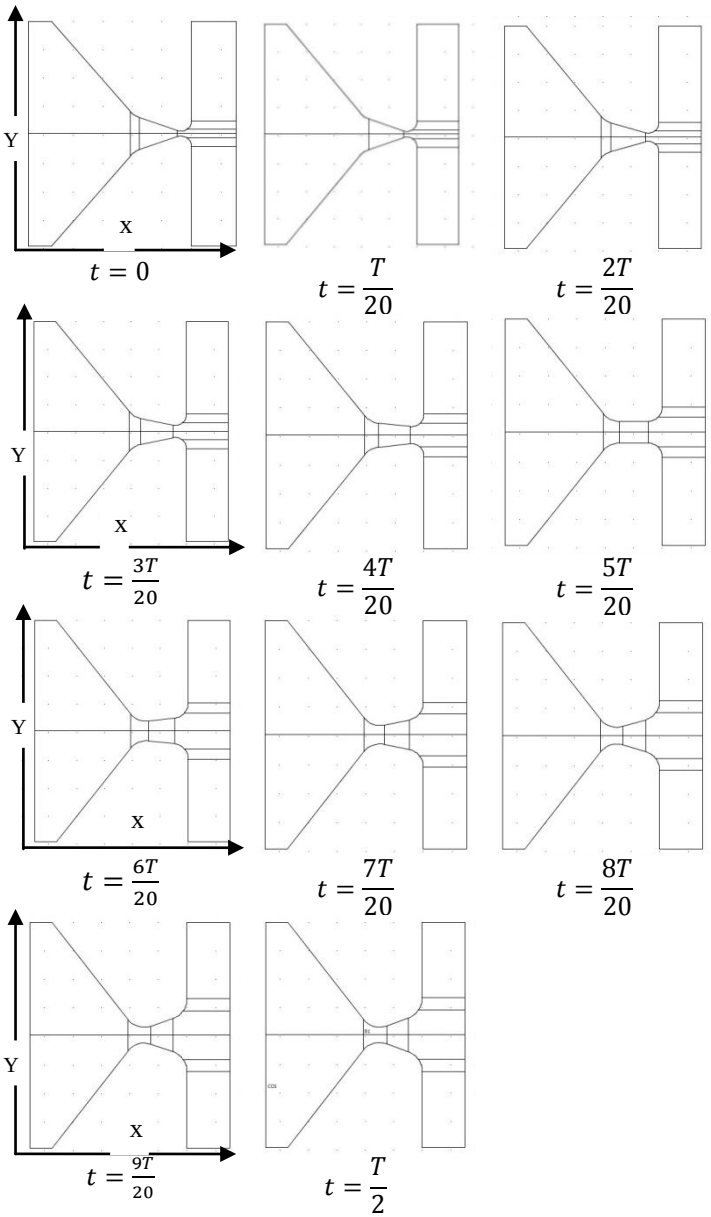

Figure 4. Glottal shape at different time values over one cycle

STEADY FLOW SIMULATIONS

Static Geometry For Different Time Steps

A series of static simulations was conducted. The glottal geometry for each static simulation was obtained from the geometry of the transient simulation at different time steps. One half of one complete oscillation cycle with period T/2 was divided into 10 intervals and the geometry of the vocal cords at each time step was saved for static simulations. All the geometries for static simulations are shown In Fig. 4.

Finite Element Solution Of Static Model

The same pressure gradient was imposed across the glottis for the dynamic and the static simulations. For steady flow simulation, the pressure is set to the desired constant magnitude at the inlet and no ramp function was used. The outlet pressure was set to be zero and the no-slip boundary condition was applied on all the other boundaries. As depicted in Fig. 4. The computational domain is divided into different subdomains for the static simulations as well.

RESULT AND DISCUSSION

In this section, fluid flow results from the dynamic model simulations are compared with those of static models with identical orifice shapes and boundary conditions. Different pressure gradients (500 and 1000 Pa) were applied across the glottis. For a pressure gradient of $\Delta P = 1000\ Pa$, a frequency of $\omega = 100\ Hz$ was used which is similar to that of actual male phonation. For the pressure gradients $\Delta P = 500 Pa$, a frequency of $\omega = 25$ is used. The pressure gradient and the stress on the walls were compared for three different configurations: convergent, parallel and divergent which correspond to included angle values of -40°, 0° and 40°, respectively.

Fourteen points are selected as virtual probes at the tip of the vocal cord. Their locations were shown in Fig. 5. The magnitudes of the shear stress and the pressure are compared at these points to quantify the differences between the dynamic and the static simulations. Normalized errors are presented in the corresponding sections.

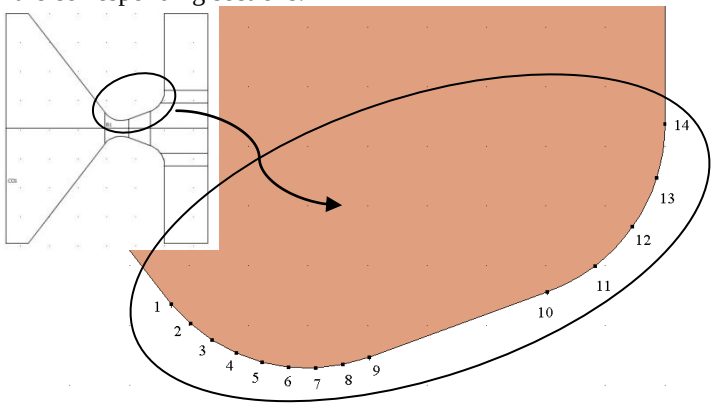

Figure 5. The location of the virtual probes on the vocal cord

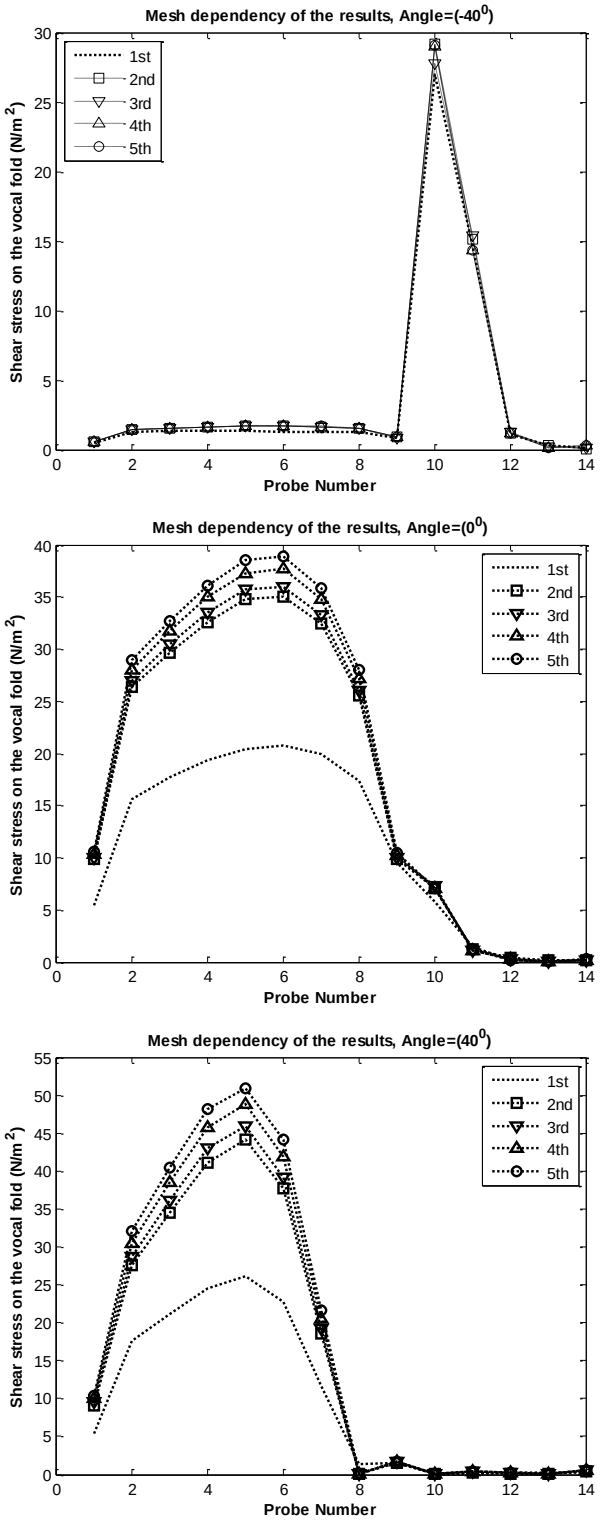

Figure 6. Mesh refinement study. Shear stress distribution for varying mesh density

After getting the preliminary results of the dynamic simulations, the mesh size in subdomains and on the boundaries are refined for 4 more steps to achieve the convergence. In the 5^{th} step, the maximum mesh size on the boundaries is 1/20 of the first simulation. In the 5^{th} step of refinement, the maximum mesh size in the glottis subdomain and on the glottis boundaries are 1/32 and 1/160 of the glottis diameter respectively. The shear stress distribution on wall is shown in Fig.6. The normalized differences between the 4^{th} and 5^{th} step of refinement using Eq. (2) is presented in Table. 1.

$$\mathbf{100} \times \frac{\sqrt{\sum\left(\boldsymbol{S}_{\boldsymbol{5th}}^{\boldsymbol{dy}} - \boldsymbol{S}_{\boldsymbol{4th}}^{\boldsymbol{dy}}\right)^{\mathbf{2}}}}{\sqrt{\sum\left(\boldsymbol{S}_{\boldsymbol{4th}}^{\boldsymbol{dy}}\right)^{\mathbf{2}}}} \tag{2}$$

Table 1. The discrepancy between the 4^{th} and 5^{th} step of mesh refinement

Ψ (°)	-40	0	40
Error (%)	0.18	3.06	4.89

Pressure Gradient

The pressure drop across the glottis for three different included angles is shown in Fig. 7 for static and dynamic cases, with $\Delta P = 1000\ Pa$. The static pressure distributions in the static models are very similar to those in the dynamic ones. Among the three different configurations, the best match was obtained for the parallel vocal fold configuration. This confirms previous observations on the validity of the quasi-steady approximation during the opening phase of the glottal duty cycle, far from onset and shut off. For the dynamic and static solution the pressures on the tip of the vocal cord are shown in Fig. 8 . The discrepancies between the dynamic and the static results are normalized using Eq. (3) and presented in Table. 2.

$$\mathbf{100} \times \frac{\sqrt{\sum\left(\boldsymbol{P}^{\boldsymbol{dy}} - \boldsymbol{P}^{\boldsymbol{st}}\right)^{\mathbf{2}}}}{\sqrt{\sum\left(\boldsymbol{P}^{\boldsymbol{st}}\right)^{\mathbf{2}}}} \tag{3}$$

Table 2. The discrepancy between the pressure of the dynamic and the static solution

Ψ (°)	-40	0	40
Error (%)	1.09	1.33	2.88

It is seen that the error is minimum for angle 0° and maximum for angle 40°.

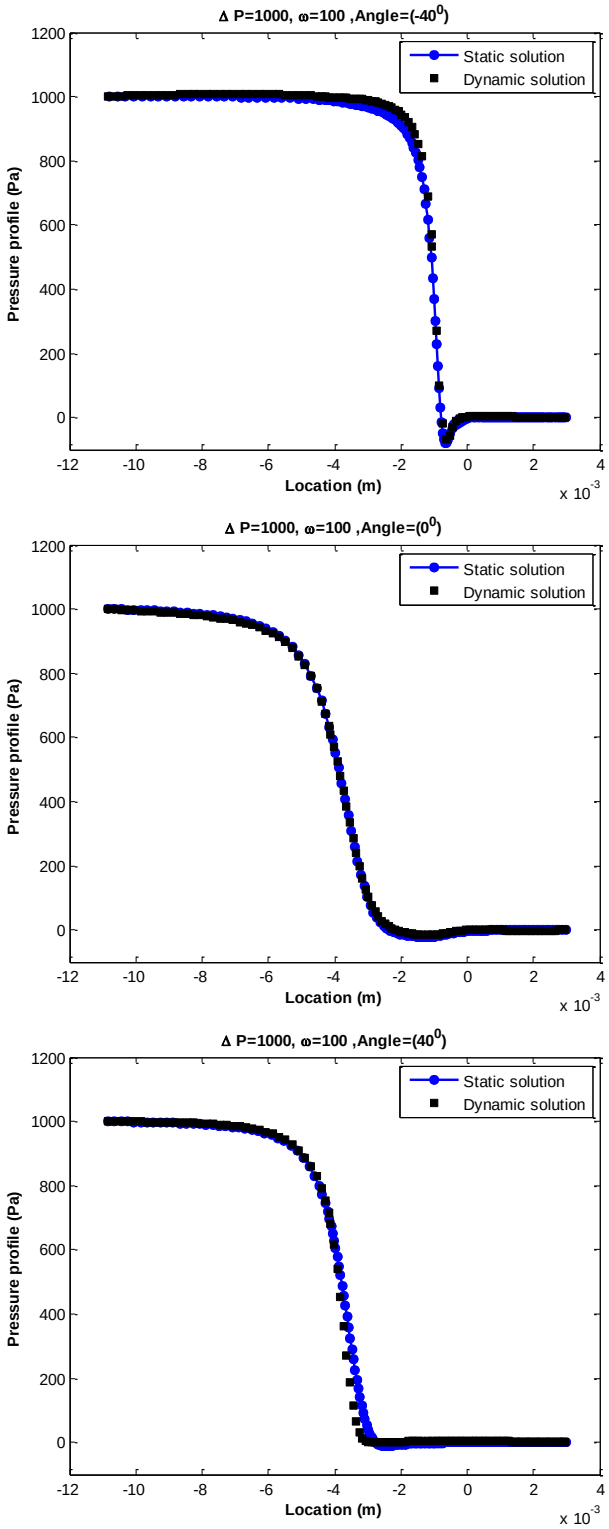

Figure 7. Pressure distribution along the glottis wall for $\Delta P = 1000$ Pa. -●-:static result, ■: dynamic result

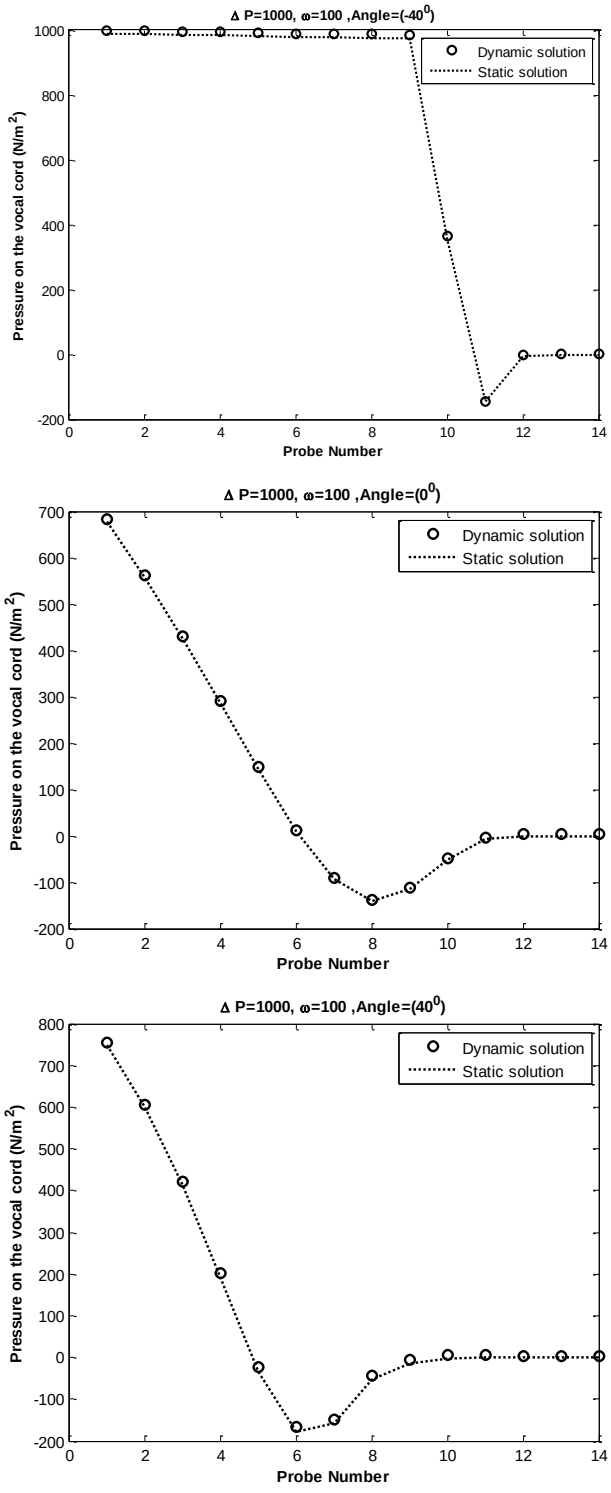

Figure. 8. Pressure distribution around the tip of the vocal cord ,○:Dynamic result, ….:static result

Stress On The Glottal Wall

The total stress on the vocal fold wall is important to compute the forces acting on the wall. The x-component of the total stress profiles are shown in Fig. 9 for pressure gradients $\Delta P = 500Pa$, $\omega = 25$.

As shown in the diagrams, the differences between the dynamic and static profiles are negligible. These results support the validity of the quasi steady approximation. For quantification of the differences of the force on the vocal cord, shear stress was recorded for the 14 locations on the wall. The results are presented in the following section

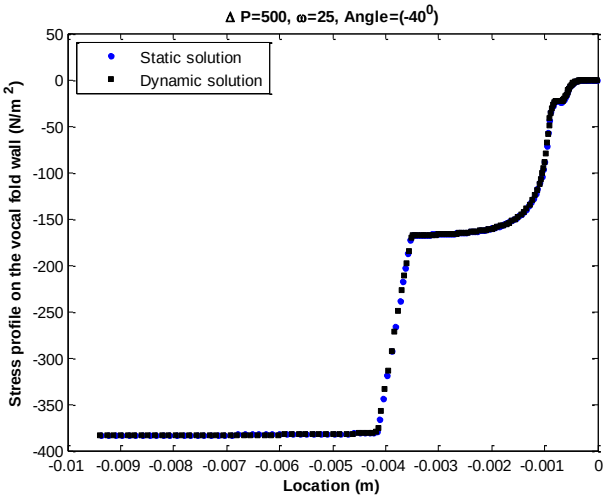

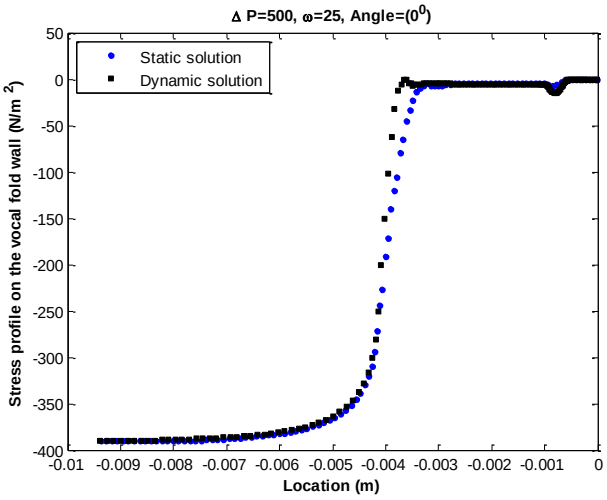

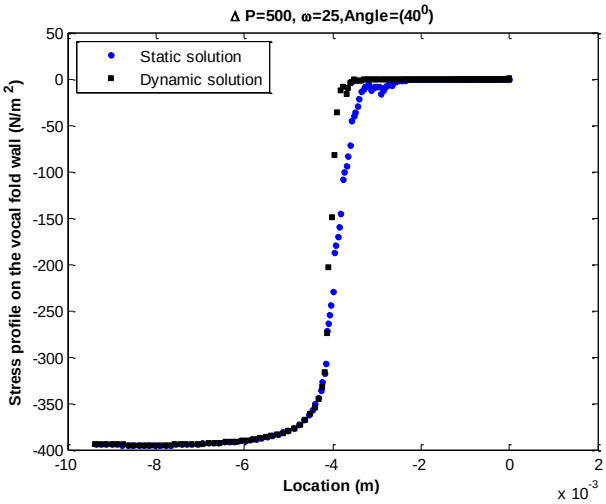

Figure 9. Component of the total stress parallel to the centerline velocity on vocal cord, for$\Delta P = 500$ Pa. ●:static results, ■: dynamic result

Shear Stress On The Glottal Wall

Shear stresses on the tip of the vocal cord at all 14 locations are shown in Fig. 10. The depicted results are for $\Delta P = 1000Pa$ and $\omega = 100$.

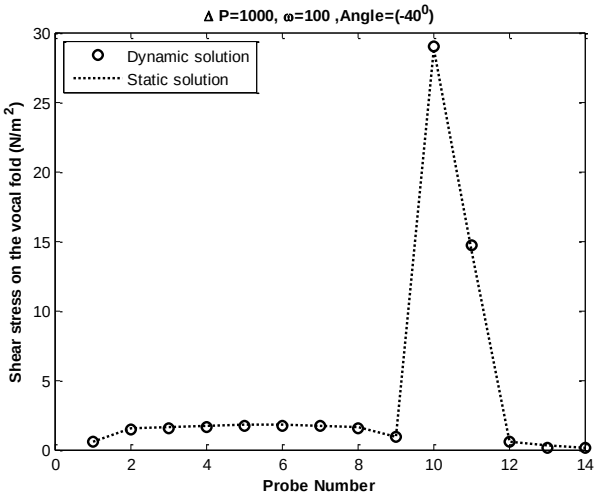

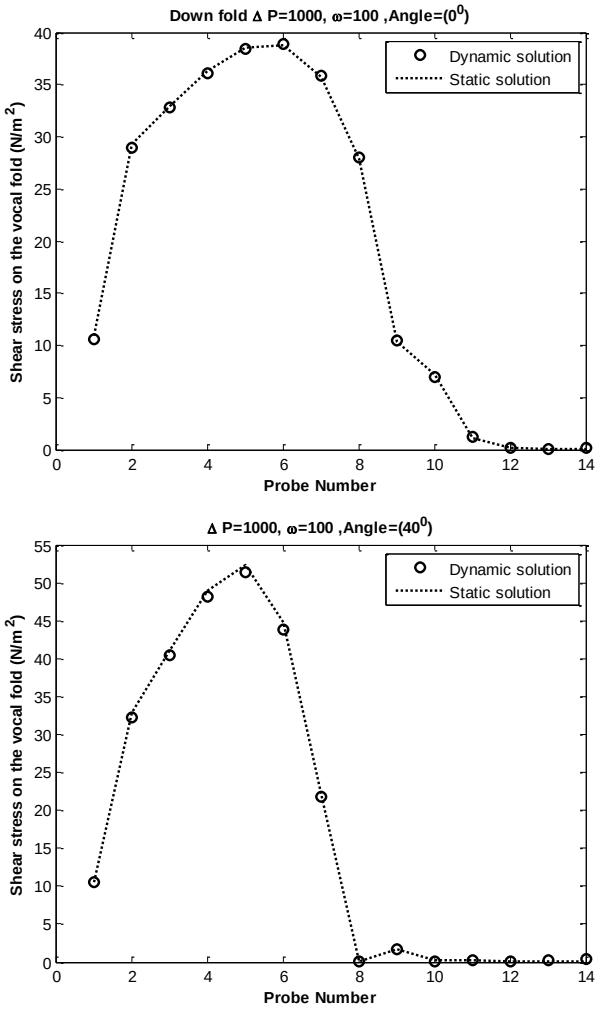

Figure. 10. Shear stress on the tip of the vocal cord ,○:Dynamic result, ….:static result

The discrepancies between the dynamic and static results are normalized using Eq. (4) and presented in Table. 3.

$$\mathbf{100} \times \frac{\sqrt{\sum\left(\boldsymbol{S^{dy}} - \boldsymbol{S^{st}}\right)^2}}{\sqrt{\sum\left(\boldsymbol{S^{st}}\right)^2}} \tag{4}$$

Table 3. The discrepancy between the shear stress of the dynamic and the static solution			
Ψ (°)	-40	0	40
Error (%)	1.78	0.64	1.90

The minimum error is for the parallel configuration and the maximum is related to the divergent configuration.

Flow Rate

The flow rate at the discharge boundary for both the dynamic and the static model for $\Delta P = 1000\,Pa$ is shown in Fig. 11. For dynamic models over one complete oscillation consists the included angle varied from -40° to 40° and then from 40° to -40°. The static flow rates are in good agreement with the dynamic ones. It is seen that over one complete cycle, the static flow rates are between the dynamic ones for the opening and the closing phase. The difference between the flow rate of the dynamic and the static solution is normalized using Eq. (5).

$$\mathbf{100} \times \frac{\sqrt{\sum\left(\boldsymbol{Q^{dy}} - \boldsymbol{Q^{st}}\right)^2}}{\sqrt{\sum\left(\boldsymbol{Q^{st}}\right)^2}} \tag{5}$$

The discrepancy between the flow rate of the dynamic and the static cases is 3.92%.

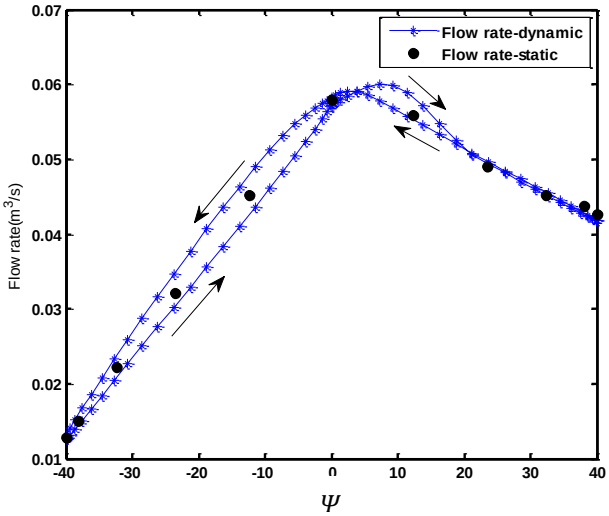

Figure 11. Flow rate vs. orifice angel over one cycle ●:static, —+—:Dynamic

Orifice Discharge Coefficient

The orifice discharge coefficient is directly correlated to the radiated sound. In the present study, the orifice coefficient is defined as the ratio of the real flow rate to the minimum area multiplied by the centerline velocity at the point of minimum area (maximum constriction) as follows:

$$C_d = \frac{Q_{real}}{(A_m \times u_m)} \tag{6}$$

The orifice discharge coefficients for the static and the dynamic cases are shown in Fig. 12.

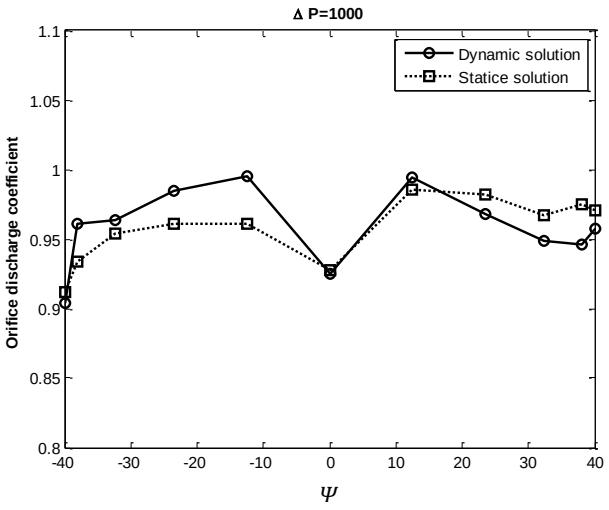

Figure 12. Orifice coefficient over half a cycle model ---□---: static , —○—: dynamic

The differences between the dynamic and static orifice coefficient is normalized as

$$\left| \frac{C_d^{dy} - C_d^{st}}{C_d^{dy}} \times 100 \right| \quad (7)$$

The maximum difference between the static and the dynamic orifice coefficient is 3.51%, which shows that quasi-steady approximation can be used with high accuracy.

CONCLUSION

To investigate the validity of the quasi-steady approximation in the glottal air flow, a series of dynamic and static Finite Element simulations of the air flow within the glottis was performed using COMSOL multiphysics software. The pressure drop across the glottis, the flow rate, shear stress and pressure on the vocal fold wall and the orifice discharge coefficient are compared in the dynamic and the static simulations. Fourteen virtual probes are located on the tip of the vocal cord to quantify the differences between the dynamic and static simulation results. Normalized discrepancy between static and dynamic solution for both pressure and the shear stress on the tip of the vocal cord is minimum for the parallel situation and maximum for divergent configuration. That is consistent with previous observations on the validity of quasi-steady approximation during the open phase of the glottal duty cycle and far from onset and shut off instances. Furthermore, it is seen that the fluid flow is less stable at the divergent configuration and the jet plum has fluctuations. These fluctuations result in higher differences between the static and dynamic solution in divergent configuration.

Although differences between the static and the dynamic simulation are observed, presented results verify the validity of quasi-steady approximation with high accuracy for the complete oscillation cycle of vocal folds.

ACKNOWLEDGMENTS

The financial support of the Canadian Institute for Health Research (CIHR) and the National Institute for Deafness and other communication disorder (NIDCD) is gratefully acknowledged.

REFERENCES

[1] Titze, I., "Principles of Voice Production. 1994," Prentice-Hall, Englewood Cliffs, NJ.

[2] Zhang, Z., Mongeau, L., and Frankel, S., 2002, "Experimental Verification of the Quasi-Steady Approximation for Aerodynamic Sound Generation by Pulsating Jets in Tubes," The Journal of the Acoustical Society of America, 112(pp. 1652.

[3] Scherer, R., Shinwari, D., De Witt, K., Zhang, C., Kucinschi, B., and Afjeh, A., 2001, "Intraglottal Pressure Profiles for a Symmetric and Oblique Glottis with a Divergence Angle of 10 Degrees," The Journal of the Acoustical Society of America, 109(pp. 1616.

[4] Šidlof, P., Švec, J., Horá Ek, J., Veselý, J., Klepá Ek, I., and Havlík, R., 2008, "Geometry of Human Vocal Folds and Glottal Channel for Mathematical and Biomechanical Modeling of Voice Production," Journal of biomechanics.41,pp.985-995

[5] Vilain, C., Pelorson, X., Fraysse, C., Deverge, M., Hirschberg, A., and Willems, J., 2004, "Experimental Validation of a Quasi-Steady Theory for the Flow through the Glottis," Journal of Sound and Vibration, 276(3-5), pp. 475-490.

[6] Pelorson, X., Hirschberg, A., Van Hassel, R., Wijnands, A., and Auregan, Y., 1994, "Theoretical and Experimental Study of Quasisteady Flow Separation within the Glottis During Phonation. Application to a Modified Two Mass Model," The Journal of the Acoustical Society of America, 96(pp. 3416).

[7] Mongeau, L., Franchek, N., Coker, C., and Kubli, R., 1997, "Characteristics of a Pulsating Jet through a Small Modulated Orifice, with Application to Voice Production," The Journal of the Acoustical Society of America, 102(pp. 1121.

[8] Kucinschi, B., Scherer, R., Dewitt, K., and Ng, T., 2006, "An Experimental Analysis of the Pressures and Flows within a Driven Mechanical Model of Phonation," The Journal of the Acoustical Society of America, 119(pp. 3011.

[9] Krane, M., and Wei, T., 2006, "Theoretical Assessment of Unsteady Aerodynamic Effects in Phonation," The Journal of the Acoustical Society of America, 120(pp. 1578.

[10] Krane, M., Barry, M., and Wei, T., 2007, "Unsteady Behavior of Flow in a Scaled-up Vocal Folds Model," The Journal of the Acoustical Society of America, 122(pp. 3659.

[11] J Sarrate, A. H., J Donea, "Arbitrary Lagrangian–Eulerian Formulation for Fluid–Rigid Body Interaction," Computer Methods in Applied Mechanics and Engineering, 190(24-25).

[12] P. Kjellgren, J. H., "An Arbitrary Lagrangian-Eulerian Finite Element Method " Computational Mechanics, 21(Number 1), pp. 81-90.